JOURNAL OF Materials CHEMISTRY

Cationic distribution in the $Li_{1-z}(Ni_{1-y}Fe_y)_{1+z}O_2$ electrode materials

G. Prado,[a] E. Suard,[b] L. Fournes[a] and C. Delmas*[a]

[a]*Institut de Chimie de la Matière Condensée de Bordeaux-CNRS and Ecole Nationale Supérieure de Chimie et Physique de Bordeaux, Château de Brivazac, Av. Dr A. Schweitzer, 33608 Pessac cedex, France. E-mail: delmas@icmcb.u-bordeaux.fr; Fax: 33 (0) 5 56 84 66 34; Tel: 33 (0) 5 56 84 62 96*

[b]*Institut Laue-Langevin, Avenue des Martyrs, BP156 38042 Grenoble cedex, France*

Received 13th April 2000, Accepted 2nd August 2000
First published as an Advance Article on the web 25th September 2000

Various $Li_{1-z}(Ni_{1-y}Fe_y)_{1+z}O_2$ materials ($0<y\leqslant 1$) were prepared and characterized by XRD. Phases with a quasi-lamellar O3 type structure are obtained only for $y\leqslant 0.30$. In order to precisely determine the cationic distribution in the layered phases, a combined analysis by X-ray and neutron diffraction, magnetic measurements and also Mössbauer spectroscopy was performed. The Rietveld refinement of the XRD patterns shows that a significant amount of 3d cation is always present in the lithium site leading to the formation of ferrimagnetic clusters. A comparative ^{57}Fe Mössbauer study of iron substituted lithium and sodium nickelate showed that the quadrupolar splittings are very sensitive to the nature of the iron site. For the largest y and z values iron ions are simultaneously present in the slab and in the interslab space.

Introduction

$LiNiO_2$ is one of the best materials proposed as a positive electrode in lithium-ion batteries. This material always presents a lithium deficiency compensated by the presence of extra Ni^{2+} ions in the lithium site. This non-stoichiometry, due to the relative stability of Ni^{2+} ions compared to Ni^{3+} ones, significantly damages the charge and discharge characteristics of the samples. Partial substitution of 3d transition metals (Co,[1–3] Mn[4,5] and Fe[6–8]) for nickel in lithium nickelate was studied in order to stabilize the 2D character and also to reduce the cost of the materials. However, cobalt remains up to now the best candidate. Indeed, for a cobalt amount close to 30%, a pure lamellar structure[9] is obtained with good electrochemical properties.[10] Nevertheless, other cations like Al[11,12] and Mg[13] can also be substituted for nickel in order to increase the thermal stability and to minimize the fading.

Concerning iron substitution, Reimers *et al.*[7] reported, for materials prepared by solid state reaction (oxide and nitrate methods) at 700 °C under dry air, that the lamellar structure of the initial $LiNiO_2$ system is preserved only in the 0–23% iron substitution range, whereas an ion exchange reaction in the 360–400 °C temperature range allowed Kanno *et al.* to extend the solid solution over the whole composition range.[8] Nevertheless, according to these authors, whatever the synthesis conditions employed, the presence of iron ions does not suppress the disordering (extra-3d metal in the lithium site) in the structure and degrades the cell capacity compared to the $LiNiO_2$ system.

However, from a fundamental point of view, iron substituted phases are interesting since iron constitutes a local probe for Mössbauer spectroscopy which gives information on the oxidation state, on the local environment and on the charge distribution around the probe. In the scope of our general studies on substituted lithium nickel oxide, a general overview of the iron substituted phases has been undertaken. Preliminary results have already been reported.[6] In this paper, the $Li_{1-z}(Ni_{1-y}Fe_y)_{1+z}O_2$ system is studied from the structural point of view. Combination of X-ray and neutron diffraction, magnetism measurements and also Mössbauer spectroscopy allowed us to obtain a good insight of the cationic distribution in this system. By comparison with reference materials like α-$NaFeO_2$ and $NaNi_{0.70}Fe_{0.30}O_2$ with a strict 2D structure, the Mössbauer study allowed us to determine the distribution of the iron ions over the different sites of the structure.

Experimental

The various iron substituted lithium nickelate samples were prepared by a coprecipitation process in aqueous solution in order to obtain homogeneous mixtures.[14] A lithium and ammonium hydroxide solution was added to a nickel and iron nitrate solution in the appropriate molar ratio. The mixture was evaporated at 90 °C under vacuum and dried at 110 °C for 15 h. The resulting powder was calcinated at 750 °C under dry oxygen for 5 h. The iron substituted sodium nickelates were prepared by solid state reaction between appropriate molar ratios of NiO, Fe_2O_3 and Na_2O_2 with a nominal ratio Na/M = 1.05 (M = Ni + Fe). For the $NaNi_{0.70}Fe_{0.30}O_2$ phase, the mixture was treated thermally at 800 °C for 15 h whereas for the pure α-$NaFeO_2$ one, the synthesis temperature was reduced to 600 °C for 24 h in order to avoid the formation of the β-$NaFeO_2$ impurity phase (high temperature form of $NaFeO_2$).[15] Only natural iron was present in the nitrate and iron oxide precursors. For all materials chemical analyses were performed by ICP. In all cases, the results confirm, from a general point of view, the chemical formula found by XRD or neutron diffraction, but they do not allow one to determine precisely the exact departure from the ideal stoichiometry.

XRD patterns were obtained using a Philips powder diffractometer PW 3040 X'pert MBP (Cu Kα radiation) equipped with a diffracted beam curve graphite monochromator. The data were collected in the 10–120° (2θ) range by 0.02° (2θ) steps with a constant counting time of 30 s. A special air-tight holder, prepared under an argon atmosphere, was used for XRD data acquisition of the sodium phases in order to

DOI: 10.1039/b002975k

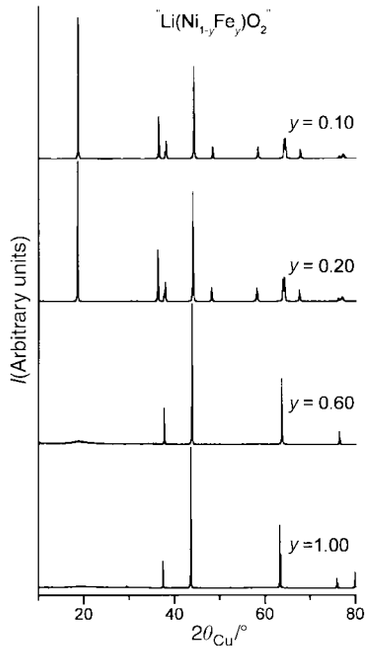

Fig. 1 XRD patterns of various "$Li(Ni_{1-y}Fe_y)O_2$" phases ($y=0.10$, 0.20, 0.60, 1.00).

prevent any reaction with air moisture. Rietveld refinements were performed using the Fullprof program.[16]

The neutron diffraction experiment was carried out on the high-resolution two-axis D2B diffractometer of the Institut Laue-Langevin. The sample was contained in a vanadium tube with a diameter of 8 mm. The diffraction pattern ($\lambda=1.5939$ Å) was collected from 1° to 160° (2θ) with 0.05° (2θ) step and a total counting time of 6 h. The Rietveld method (Fullprof program) was used for the structure refinement. The neutron scattering lengths b_i ($\times 10^{-12}$ cm) were $b_{Li}=-0.19$, $b_{Ni}=1.03$, $b_{Fe}=0.954$ and $b_O=0.5803$.

Magnetic susceptibility measurements were obtained with an automatic susceptometer (DSM8-Manics) between 5 K and 300 K. All data were corrected for diamagnetism.

Mössbauer spectra were recorded at room temperature with a constant acceleration spectrometer using a ^{57}Co source in a Rh matrix. The velocity was calibrated using pure iron metal as a standard material.

Results

X-Ray diffraction patterns study

The $Li(Ni_{1-y}Fe_y)O_2$ nominal composition system was investigated for various amounts of iron ($0<y\leqslant 1$). Fig. 1 shows the evolution of the XRD patterns with y; three domains can be considered, in agreement with Reimers *et al.*:[7]

(1) for the smallest iron amounts ($0\leqslant y\leqslant 0.30$), pure phases crystallizing in the rhombohedral system with the $R\bar{3}m$ space group as the $LiNiO_2$ system are obtained,

(2) for the iron rich compositions ($y>0.50$), the materials crystallize in the cubic system (with the rocksalt structure) as the α-$LiFeO_2$ end member. Nevertheless, at low angle ($2\theta_{Cu}\approx 18°$), a weak and broad line, corresponding to the position of the (003) line of the layered phases, remains. It could be attributed to short range ordering, as already evidenced in α-$LiFeO_2$.[17–19]

(3) in the $0.30<y<0.50$ domain, the cubic and the lamellar phases coexist (not shown in Fig. 1).

Note that only lamellar phases are interesting from the electrochemical point of view and therefore, in the following section, our interest was focused on these materials.

The α-$NaFeO_2$ and $Na(Ni_{0.70}Fe_{0.30})O_2$ materials are also pure phases which crystallise in the rhombohedral system (S. G.: $R\bar{3}m$) and their XRD patterns (not shown here) are in good agreement with the literature.[20–22]

Table 1 Refined parameters and reliability factors obtained from XRD pattern Rietveld refinement of the $Li_{0.92}(Ni_{0.80}Fe_{0.20})_{1.08}O_2$ phase[a]

Atom	Site	Wyckoff positions			Occupancy	B/Å^2
Li(1)	3b	0	0	1/2	0.916(7)	2.3(6)
Ni/Fe(1)	3b	0	0	1/2	$z=0.084(7)$	$=B$(Li)
Ni/Fe(2)	3a	0	0	0	1.000	0.30(7)
O(1)	6c	0	0	$z_{ox.}=0.2561(5)$	1.000	0.48(14)

Conditions of the run	
Temperature	300 K
Angular range	$10°\leqslant 2\theta\leqslant 120°$
Step scan increment (2θ)	0.02°
Zero point (2θ)	−0.0062(2)°
Number of fitted parameters	14
Profile parameters	
Pseudo-Voigt function	
$PV=\eta L+(1-\eta)G$	$\eta_0=0.467(53)$
with $\eta=\eta_{0°}+X(2\theta)$	
	$X=0.001(1)$
Halfwidth parameters	$U=0.026(7)$
	$V=0.0117)$
	$W=0.008(1)$

Conventional Rietveld *R*-factors for points with Bragg contribution
$R_{wp}=11.0\%$; $R_B=3.9\%$

[a] $Li_{1-z}(Ni_{0.80}Fe_{0.20})_{1+z}O_2$: Space group: $R\bar{3}m$; Constraints: $n(Li)_{3b}+n(Ni/Fe)_{3b}=1$, $B(Li)_{3b}=B(Ni/Fe)_{3b}$; $a_{hex.}=2.8955(1)$ Å; $c_{hex.}=14.3017(9)$ Å; Standard deviations have been multiplied by the Scor parameter (=3.4) to correct local correlations.[16]

X-Ray diffraction analysis of the layered phases. The structure of $LiNi_{1-y}Fe_yO_2$ ($y=0.10$, 0.20, 0.30) nominal composition materials was characterized by Rietveld refinement of their XRD patterns using the method described for the $Li_{1-z}Ni_{1+z}O_2$ system.[23] In order to study a more lithium deficient phase, a sample with $y=0.20$ and with an initial Li/M ratio equal to 0.85 (M=Ni+Fe) was synthesized and characterized by the same method. This study was extended to the α-$NaFeO_2$ and $NaNi_{0.70}Fe_{0.30}O_2$ phases which were also used as reference materials for the Mössbauer study.

The results of the refinement obtained for the $y=0.20$ phase with a nominal ratio Li/M=1 are gathered as an example in Table 1. The corresponding observed and calculated profiles are compared in Fig. 2. A general comparison of all the structural data of the various materials is reported in Table 2.

(1) For the series of $Li(Ni_{1-y}Fe_y)O_2$ materials synthesized

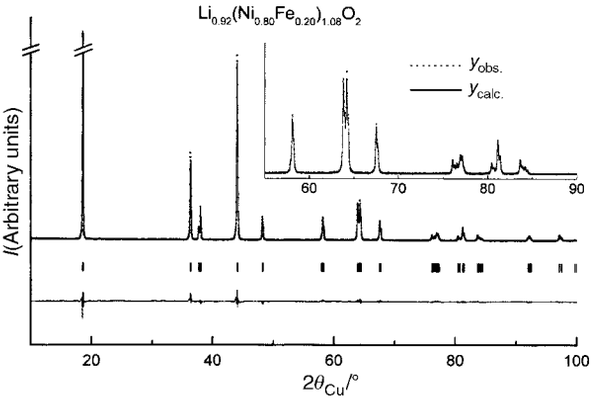

Fig. 2 XRD pattern of the $Li_{0.92}(Ni_{0.80}Fe_{0.20})_{1.08}O_2$ phase. The difference between the observed and calculated patterns is given. The vertical bars show the Bragg reflections. The 100–120° (2θ) domain is not shown. A closeup of the XRD pattern in the 55–90° (2θ) range is given in the inset.

Table 2 Structural parameters of the various $Li_{1-z}(Ni_{1-y}Fe_y)_{1+z}O_2$ ($y=0.10$, 0.20, 0.30) and $NaNi_{1-y}Fe_yO_2$ ($y=1$, 0.30) phases deduced from XRD pattern Rietveld refinement[c]

	Li/M nominal (M = Ni, Fe)	$a_{hex.}$/Å	$c_{hex.}$/Å	$z_{ox.}$[a]	z[b]	R_B (%)	R_{wp} (%)	$d_{(M-O)}$/Å (M = Ni, Fe)	$d_{(Li-O)}$/Å	c/a
$Li_{1-z}(Ni_{0.90}Fe_{0.10})_{1+z}O_2$	1.00	2.8903(1)	14.2607(7)	0.2581(3)	0.061(3)	1.4	7.6	1.983(2)	2.118(3)	4.93
$Li_{1-z}(Ni_{0.80}Fe_{0.20})_{1+z}O_2$	1.00	2.8955(1)	14.3017(9)	0.2561(5)	0.084(7)	3.9	11.0	2.003(1)	2.105(4)	4.93
$Li_{1-z}(Ni_{0.80}Fe_{0.20})_{1+z}O_2$	0.85	2.9003(1)	14.3142(11)	0.2568(4)	0.145(5)	3.8	11.0	2.001(3)	2.114(4)	4.93
$Li_{1-z}(Ni_{070}Fe_{0.30})_{1+z}O_2$	1.00	2.9008(1)	14.3417(15)	0.2567(4)	0.074(5)	3.6	15.9	2.003(3)	2.115(4)	4.94
α-$NaFeO_2$	1.05	3.0239(1)	16.0882(9)	0.2651(7)	—	9.7	19.2	2.061(6)	2.357(7)	5.32
$Na(Ni_{0.70}Fe_{0.30})O_2$	1.05	2.9719(1)	15.8523(9)	0.2674(6)	—	6.5	15.9	2.008(5)	2.345(6)	5.33

[a] $z_{ox.}$ is the position of the oxygen atom in the structure. [b] z is the amount of the extra-3d metal ions in the lithium layer. [c] Standard deviations have been multiplied by the Scor parameter given for each Rietveld refinement to correct local correlations.[16]

with Li/M = 1, an increase of the $a_{hex.}$ and $c_{hex.}$ parameters with increasing y is observed, due to the larger size of the Fe^{3+} ions (0.645 Å) compared to the Ni^{3+} ones (0.56 Å).[24] Moreover, the materials exhibit the $Li_{1-z}(Ni_{1-y}Fe_y)_{1+z}O_2$ formula with a significant departure from ideal stoichiometry. The amount of z extra-3d metal ions in the interslab space is almost the same ($0.06 \leqslant z \leqslant 0.08$) although the iron ratio increases.

(2) For the sodium phases, the cell parameters are in good agreement with those from the literature.[21,22] The large difference in size between the nickel and iron ions and the sodium one induces a strict bidimensional structure. Indeed, the c/a ratio, whose departure from the 4.90 value (theoretical value for cubic symmetry) indicates the tendency to form a bidimensional structure, is significantly larger for the sodium phases. The M–O bond distance in the $Na(Ni_{0.70}Fe_{0.30})O_2$ phase is very similar to that of the $Li_{0.93}(Ni_{0.70}Fe_{0.30})_{1.07}O_2$ phase since they have the same slab composition. For α-$NaFeO_2$ the M–O bond distance is larger due to the large size of iron ions.

Note that, due to the very weak scattering factor of Li, only the amount of (Ni,Fe) ions in the lithium site was refined, the lithium content within the lithium layer being simply deduced from the crystallographic formula. For the same reason, the presence of lithium in the (Ni,Fe) layer is very difficult to determine from XRD data: it is the neutron diffraction powder patterns that provide direct information on the amount of lithium ions in the two types of sites.

Table 3 Refined parameters and reliability factors obtained from the Rietveld refinement of the $Li_{0.86}(Ni_{0.80}Fe_{0.20})_{1.14}O_2$ neutron diffraction pattern[a]

Atom	Site	Wyckoff positions	Occupancy	B/Å^2
Li(1)	3b	0 0 1/2	0.87(1)	5(2)
Ni/Fe(1)	3b	0 0 1/2	$z=0.13(1)$	$=B$(Li)
Ni/Fe(2)	3a	0 0 0	0.97(2)	0.55(6)
Li(2)	3a	0 0 0	0.03(2)	$=B$(Ni/Fe)
O	6c	0 0 $z_{ox.}=0.2570(2)$	1.000	0.89(9)

Conditions of the run

Temperature	300 K
Angular range	$0° \leqslant 2\theta \leqslant 160°$
Channel increment (2θ)	0.05°
Zero point (2θ)	0.049(2)
Number of fitted parameters	16
Absorption coefficient (μR)	0.6590

Profile parameters

Pseudo-Voigt function	
$PV=\eta L+(1-\eta)G$	$\eta=0.143(16)$
Halfwidth parameters	$U=0.163(6)$
	$V=-0.177(13)$
	$W=0.163(5)$

Conventional Rietveld *R*-factors for points with Bragg contribution

$R_{wp}=7.1\%$; $R_B=1.9\%$

[a] $Li_{1-z}(Ni_{0.80}Fe_{0.20})_{1+z}O_2$: Space group: $R\bar{3}m$; $a_{hex.}=2.90044(7)$ Å; $c_{hex.}=14.3155(5)$ Å; Constraints: $n(Li)_{3b}+n(Ni/Fe)_{3b}=1$, $B(Li)_{3b}=B(Ni/Fe)_{3b}$, $n(Ni/Fe)_{3a}+n(Li)_{3a}=1$, $B(Ni/Fe)_{3a}=B(Li)_{3a}$. Standard deviations have been multiplied by the Scor parameter ($=2.4$) to correct local correlations.[16]

Neutron powder diffraction analysis of the lithium deficient $y=0.20$ phase. The negative coherent scattering length (b) of Li allows one to refine its amount in the (Ni,Fe) slab since these two atoms have high positive b values. Neutron diffraction is thus complementary to XRD in characterizing the exact structure of these materials. However, note that, in any case, iron and nickel cannot be distinguished. In order to determine the possible presence of lithium ions in the 3d metal (Ni,Fe) site, neutron diffraction was performed on a $Li_{0.86}(Ni_{0.80}Fe_{0.20})_{1.14}O_2$ phase with a high departure from stoichiometry (formula determined by Rietveld refinement of XRD pattern). Indeed, previous neutron studies carried out in our lab on the $Li_{1-z}Ni_{1+z}O_2$ phases with various z values gave evidence of a few percent of Li ions (ε) in the NiO_2 slab only for high extra-nickel ion amounts ($z=0.25$, $\varepsilon \leqslant 2\%$).[25]

As in the case of XRD analyses, the structure was first refined (space group $R\bar{3}m$) with Li, Ni(Fe) and O in 3b (0,0,1/2), 3a (0,0,0) and 6c (0,0,$z_{ox.}$) sites, respectively. The isotropic atomic displacement parameters were fixed at 0.4. The refined cell and oxygen position parameters were identical to those found in the XRD refinement. Then, a partial disordering, authorizing extra-metal ions within the lithium site and lithium ions in the 3d metal layer was considered with the constraint that the total occupancy at each site be equal to 1. The site occupancies and their isotropic atomic displacement factors B were refined and are reported in Table 3. The R-factors are also given. The observed and calculated neutron diffraction profiles are displayed in Fig. 3.

Note that the isotropic atomic displacement parameter B(Li) in the lithium site has a high value with a very large standard deviation. Indeed, due to its high absorption coefficient (natural lithium was used for synthesis), accurate observation of the lithium atom remains difficult. Moreover, the layers are

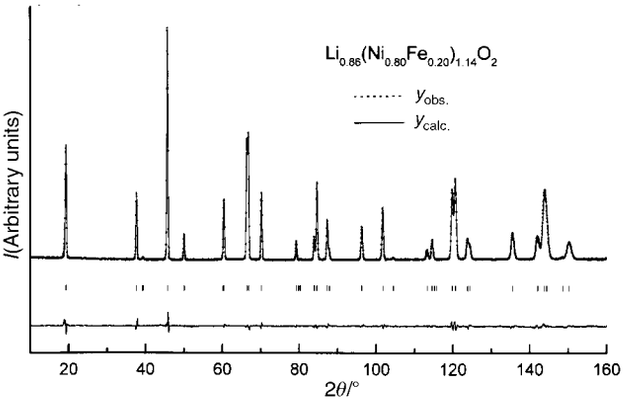

Fig. 3 Neutron diffraction pattern of the $Li_{0.86}(Ni_{0.80}Fe_{0.20})_{1.14}O_2$ phase ($\lambda=1.5939$ Å). The difference between the observed and calculated profiles is given. The vertical bars show the Bragg reflections.

corrugated at the atomic scale due to: (i) the difference in size between nickel and iron ions in metal layers and (ii) the presence of extra-3d metal ions in the lithium site which reduces locally the interslab space. Thus, the real lithium position in the structure can slightly vary from site to site, contrary to what was considered in the refinement. A very small amount (0.03) of lithium ions was found in the nickel layer. The large standard deviation shows that this result is not meaningful at the 2σ level. Therefore, one can consider that the (Ni,Fe) layer is almost ideal with a very small amount of lithium ions ($\leqslant 0.03$).

This neutron analysis is in good agreement with the latter X-ray results since z was found to be equal to 0.13 in the neutron study, *cf.* 0.14 in the XRD study (Table 2). The $Li_{1-z}(Ni_{1-y}Fe_y)_{1+z}O_2$ system presents the same behavior as the $Li_{1-z}Ni_{1+z}O_2$ one. Indeed, previous work on the $Li_{1-z}Ni_{1+z}O_2$ system proved that lithium occupancy in the nickel site could increase and become significant when increasing lithium deficiency.[25,26] Pickering *et al.* showed that for $z=0.20$, only 1% of the lithium ions were located in the nickel site.[26] For the most stoichiometric phases, no lithium ions are situated in the nickel layer. By analogy, we assume that for the $Li_{1-z}(Ni_{1-y}Fe_y)_{1+z}O_2$ system with $y=0.10$, 0.20 Li/M mixing does not occur for the lowest z values. This result may be extended to the $y=0.30$ phase. Indeed, for the 40% iron composition, coexistence of the layered and cubic phases suggests that as soon as Li/Fe mixing appears and becomes significant, a cubic phase close to α-$LiFeO_2$ is created in addition to the lamellar phase.

In conclusion, we assume that for the various iron phases considered in this paper, the amount of Li ions in the 3d metal layer is negligible compared to the 3d metal ion occupancy in the lithium site.

Magnetic susceptibility study

Numerous reports on the parent $Li_{1-z}Ni_{1+z}O_2$ materials already pointed out the relationship between the amount of extra-3d metal ions in the lithium site and the magnetic properties.[27–31] Indeed, strong antiferromagnetic interactions occur between the extra-3d metal ions and the adjacent Ni^{2+}, Fe^{3+} and Ni^{3+} ions of the slabs, leading locally to ferrimagnetic clusters. The size and the number of clusters increase with the amount of extra-3d metal ions, so that the magnetic behavior evolves from paramagnetic (or superparamagnetic) for isolated clusters to a general ferrimagnetic order when all the clusters percolate.[32] The purpose of this study is not to make an overall magnetic characterization of these materials but only to confirm the result found for the cationic distribution in the Rietveld refinement by using the sensitivity of the magnetic properties to the cluster concentration, which is directly related to the amount of 3d cations in the lithium site. We report in this paper the variation of the reprociprocal molar magnetic susceptibility *vs.* temperature only for iron substituted lithium nickelate with a quasi-lamellar structure: samples with $y=0.10$, 0.20, 0.30 and similar z amount (Fig. 4a) and 20% iron containing samples with two different z amounts (Fig. 4b). The curve relative to quasi-2D $Li_{0.98}Ni_{1.02}O_2$ is also reported in Fig. 4a for comparison.

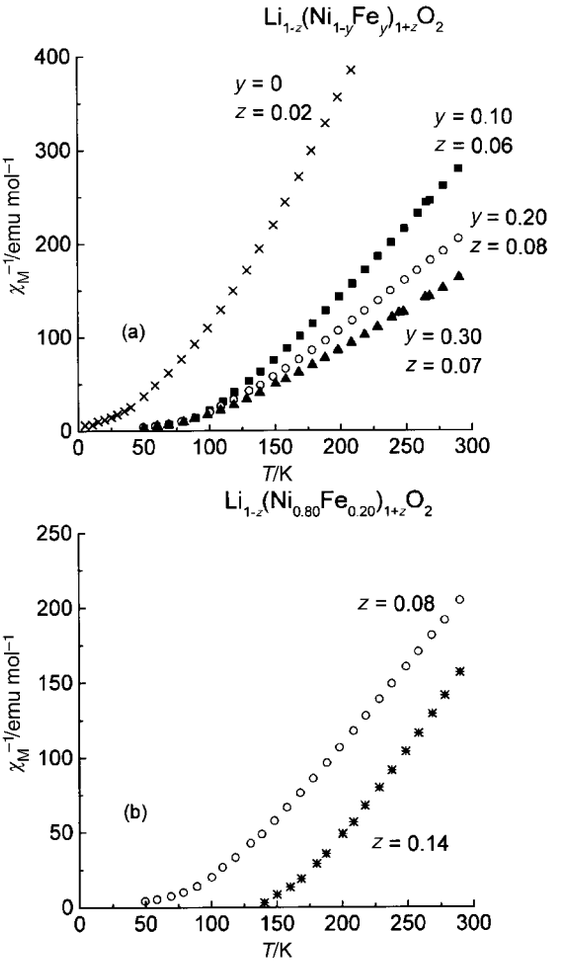

Fig. 4 Temperature dependence of the inverse of the magnetic molar susceptibility for $Li_{0.98}Ni_{1.02}O_2$ and various $Li_{1-z}(Ni_{1-y}Fe_y)_{1+z}O_2$ phases ($y=0.10$, 0.20, 0.30; $z=0.06$, 0.08, 0.07, respectively (a)); ($y=0.20$ with $z=0.08$ and 0.14 (b)).

All curves show an overall similar shape for the iron substituted phases. The reciprocal molar susceptibility decreases upon cooling and becomes equal to zero in the 50–150 K temperature range, revealing the presence of a transition temperature. The change in the curve slope in the vicinity of this temperature is weak showing the appearance of short range magnetic ordering before the long range ordering. Therefore, with such a type of curve it is very difficult to determine precisely the ordering temperature. However, comparison of the curves shows that for the $z=0.06$ and 0.08 samples the ordering temperatures are very similar, while it increases

Table 4 Comparison between the theoretical Curie constants and the inverse slopes of the $\chi^{-1}=f(T)$ curves in the 200–300 K range for the $Li_{1-z}(Ni_{1-y}Fe_y)_{1+z}O_2$ phases ($y=0.00$, 0.10, 0.20, 0.30)

$Li_{1-z}(Ni_{1-y}Fe_y)_{1+z}O_2$				
y	z	Paramagnetic ions	$C_{theor.}$	$(slope)^{-1}$ of the $\chi^{-1}=f(T)$ curve
0.00	0.02	$Ni^{2+}_{0.04}Ni^{3+}_{0.92}$	0.41	0.37
0.10	0.06	$Ni^{2+}_{0.12}Ni^{3+}_{0.83}Fe^{3+}_{0.11}$	0.90	0.69
0.20	0.08	$Ni^{2+}_{0.16}Ni^{3+}_{0.70}Fe^{3+}_{0.22}$	1.37	0.96
0.20	0.14	$Ni^{2+}_{0.28}Ni^{3+}_{0.63}Fe^{3+}_{0.23}$	1.51	0.81
0.30	0.07	$Ni^{2+}_{0.14}Ni^{3+}_{0.61}Fe^{3+}_{0.32}$	1.77	1.21

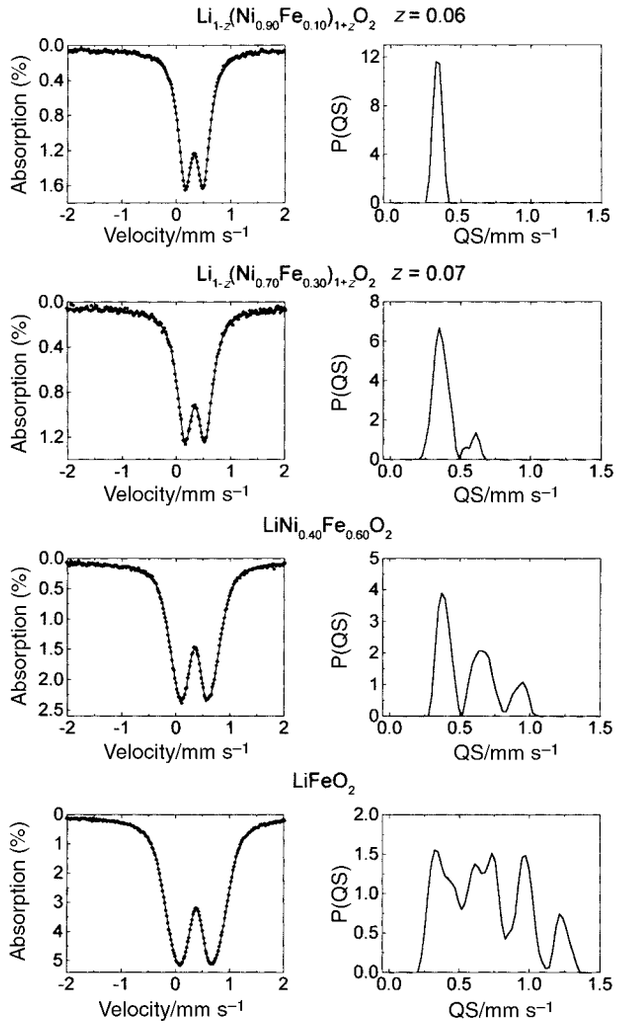

Fig. 5 Mössbauer spectra (left side) and corresponding quadrupole splittings distributions (right side) for various "$Li(Ni_{1-y}Fe_y)O_2$" phases.

considerably when the amount of extra-3d ions increases ($z=0.14$), in good agreement with previous data of the $Li_{1-z}Ni_{1+z}O_2$ system.[23,28,32] Above 200 K the reciprocal susceptibility varies almost linearly *vs.* temperature; nevertheless, the studied temperature range is too narrow to be associated unambiguously with a paramagnetic state. The theoretical Curie constant values calculated assuming the $Li_{1-z}(Ni_{1-y}Fe_y)_{1+z}O_2$ formula deduced from the XRD pattern refinements with $2z$ Ni^{2+}, $((1-y)(1+z)-2z)$ Ni^{3+} and $y(1+z)$ Fe^{3+} ions are reported in Table 4 in comparison with the inverse slope of the $\chi^{-1}=f(T)$ curve above 200 K. In fact the inverse slopes of the experimental curves are significantly smaller than the theoretical values expected in the paramagnetic state, as was observed for the ferrimagnetic $Li_{1-z}Ni_{1+z}O_2$ phases ($z\geqslant 0.06$) just above the ordering temperature.[23] In these systems the thermal variation of the susceptibility obeys the Curie–Weiss law only at high temperature (out of the range considered in the present study).[6] Such behavior must be opposed to that observed in the $Li_{1-z}(Ni_{1-y}Mg_y)_{1+z}O_2$ system with only diamagnetic Mg^{2+} in the interslab space, for which the Curie–Weiss law was obeyed at low temperature.[13] A complementary Mössbauer study at 4.2 K shows that the spectra of the iron substituted materials are constituted of six lines characteristic of a magnetically ordered phase. Nevertheless, a paramagnetic peak remains indicating superparamagnetic properties. The simultaneous presence of these two different contributions evidences the heterogeneity in the distribution of the ferrimagnetic clusters over the structure.

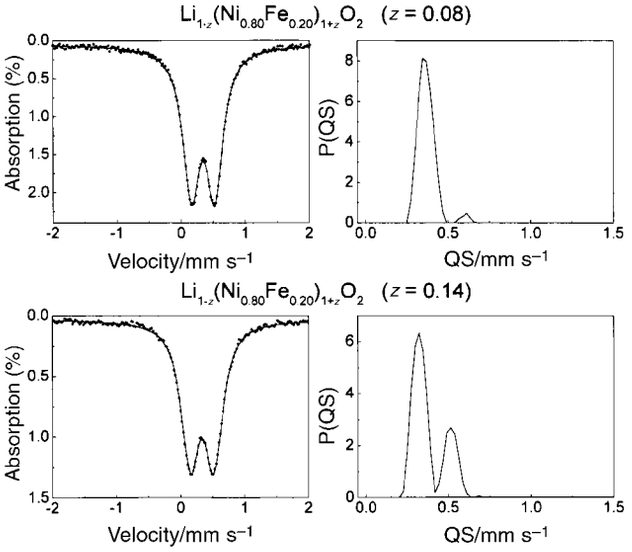

Fig. 6 Mössbauer spectra and corresponding quadrupole splitting distributions of the $Li_{1-z}(Ni_{0.80}Fe_{0.20})_{1+z}O_2$ phases ($z=0.08$, 0.14).

Fig. 4a shows that the transition temperatures of the three $Li_{1-z}(Ni_{1-y}Fe_y)_{1+z}O_2$ samples with $y=0.10$, 0.20, 0.30 are almost the same; this is in agreeement with the presence of similar 3d metal amounts in the lithium layer in the three materials, leading to equivalent amounts of ferrimagnetic domains.

Fig. 4b displays a comparison of the magnetic behavior between the two 20% iron containing samples with different z values. The $z=0.14$ sample has a much higher transition temperature than the $z=0.08$ one resulting from an increase in the number of ferrimagnetic domains when increasing the amount of metal ions in the lithium layer. As a result this magnetic study confirms in a general way the cationic distribution found in the Rietveld refinement of the XRD patterns.

Mössbauer study

We have just evidenced the presence of a significant amount of transition metal ions in the interslab space. A systematic Mössbauer study for all the materials was performed in order to discriminate between the nickel and the iron ions. Indeed, Fe^{3+} ions are substituted for nickel ones in the slab but they could also be present in the interslab space. Their size (0.645 Å), which is similar to that of Ni^{2+} (0.69 Å), suggests that they could be stabilized in the large lithium site (0.76 Å) as previously discussed by Reimers *et al.* Our study was realized by comparing the iron substituted lithium nickelates with the α-$NaFeO_2$ and $NaNi_{0.70}Fe_{0.30}O_2$ materials in which iron ions are only located in the octahedral site of the slab as evidenced by Rietveld refinement of the XRD patterns (Table 2). The room temperature Mössbauer spectra were recorded for the $LiNi_{1-y}Fe_yO_2$ phases ($y=0.10$, 0.30, 0.60, 1.00) (Fig. 5), for $Li_{1-z}(Ni_{0.80}Fe_{0.20})_{1+z}O_2$ samples with $z=0.08$ and 0.14 (Fig. 6), and also for the α-$NaFeO_2$ and $NaNi_{0.70}Fe_{0.30}O_2$ phases (Fig. 7).

All Mössbauer spectra primarily consist of a symmetric single quadrupole doublet. A first mathematical treatment assuming each spectrum as a sum of Lorentzian peaks shows that only Fe^{3+} ions in the high spin state are present. Nevertheless, an increase of the FWHM of the Mösbauer line with increasing iron amount is observed. In these layered structures, the existence of a distribution of local environments around the iron ions leading to a distribution of quadrupole splittings can explain this behavior. In consequence, the Mössbauer spectra were fitted to a sum of quadrupole splittings with their relative probability as free parameters and with the linewidth fixed at

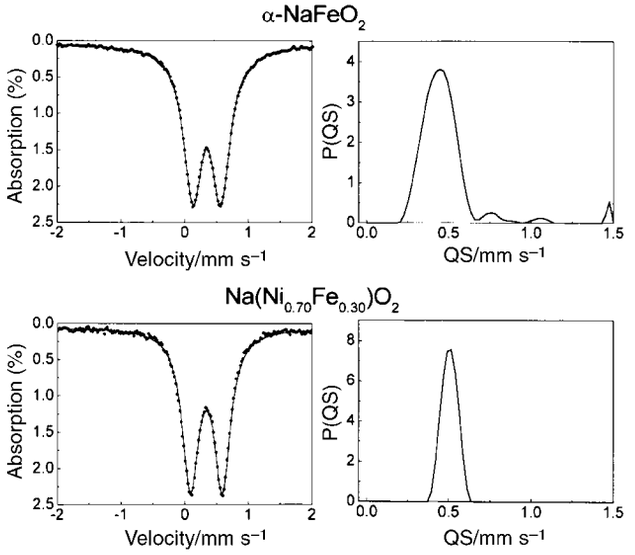

Fig. 7 Mössbauer spectra and corresponding quadrupole splitting distributions of the α-$NaFeO_2$ and $NaNi_{0.70}Fe_{0.30}O_2$ phases.

the classical value ($\Gamma = 0.30$ mm s^{-1}) for the ^{57}Fe isotope and the isomer shift of each phase fixed at the value preliminarily determined in the first mathematical treatment. Table 5 summarizes the isomer shift and the average quadrupole splitting values thus obtained for all the materials. These parameters are characteristic of trivalent iron ions in the high spin (HS) state in a distorted octahedral surrounding,[22] which is in good agreement with the X-ray structural characterization results. Owing to the exclusive presence of HS Fe^{3+} ions, the quadrupole splitting (QS) arises only from lattice contribution to the electric field gradient at the iron sites. The increase of QS is therefore related to the increase of the distortion in the [FeO_6] octahedra and to the nature, the charge and the distribution of the first cationic neighbors.

Note that the line broadening of the spectra should be also treated as a sum of single peaks with no quadrupole splitting but with a distribution of isomer shifts or a situation with a simultaneous variation of the quadrupole splittings and isomer shifts since they are not independent parameters. However, we experimentally observed that the isomer shift does not vary perceptibly with the increase of iron amount in the material and with the structural changes (0.33–0.38 mm s^{-1}) contrary to the average quadrupole splitting (0.33–0.69 mm s^{-1}) (Table 5). Indeed, since, for all the materials, trivalent iron ions are in octahedral surroundings, we assume that the modification of the cationic environment of the iron ions with increasing iron content or upon structural modification does not change perceptibly the nature of the iono-covalent character of the M–O bond, which fixes the isomer shift parameter. Therefore, one can consider that the isomer shift only reflects, in this study, the oxidation state and the electronic configuration of the iron ion, its spin state and its coordination. On the contrary, the various cationic environments become more asymmetric and lead to a large increase in the average quadrupole splitting. These observations validate the approximation made in the spectra calculation since the results give a rough estimate of the chemical and physical reality.

The resulting distributions of quadrupole splittings are shown on the right side of Fig. 5 which gives the relative populations of iron ions for each value of quadrupole splitting. In all cases, discrete distributions are obtained; this behavior is characteristic of a definite number of unusual iron ion environments in the structure. For rhombohedral phases, one or two peaks with different average values are present in the obtained distributions, whereas cubic phases exhibit an increasing number of unusual environments, the number of peaks increasing with the disorder in the structure. The distributions obtained (Fig. 6) for both $Li_{1-z}(Ni_{0.80}Fe_{0.20})_{1+z}O_2$ materials with $z = 0.08$ and 0.14 are discrete ones with one predominating peak at low quadrupole splitting and a second one (at higher quadrupole splitting) which rises when increasing the z value, *i.e.* with the loss of lamellar character.

Discussion

In order to characterize the cationic distribution in the $Li_{1-z}(Ni_{1-y}Fe_y)_{1+z}O_2$ ($0 < y \leqslant 0.30$) phases, the relation between the structure and the Mössbauer spectra of sodium and cubic phases is discussed in a first step. These two families can be considered as reference materials from this point of view.

2D α-$NaFeO_2$ and $NaNi_{0.70}Fe_{0.30}O_2$ phases

As previously mentioned in the XRD characterization section, these two materials exhibit strictly layered structures due to the difference in size between the transition metal ions and the sodium ones which prevents local disordering. As shown in Fig. 7, for both materials, the distribution of quadrupole splittings exhibits only one peak. This indicates that there is only one type of environment for iron ions as expected from the structure. In the case of the pure iron phase, the distribution is larger than in the mixed $NaNi_{0.70}Fe_{0.30}O_2$ phase; this behavior is not explained. However, the existence of only one distribution of quadrupole splittings for the latter material shows that the difference between the various possible Ni^{3+} and Fe^{3+} ion distributions around the Fe^{3+} ion, acting as the Mössbauer probe, is too small to induce significant changes in the quadrupole splitting. A schematic representation of the iron environment in the structure is shown in Fig. 8. The iron ion in its oxygen octahedron is surrounded by six transition metal

Table 5 Mössbauer parameters and usual fit parameters for the various lithium and sodium phases[a]

	IS/mm s^{-1}	$\overline{QS}$/mm s^{-1}	Misfit	χ^2
$LiNi_{0.90}Fe_{0.10}O_2$	0.33	0.33	0.02	0.85
$LiNi_{0.80}Fe_{0.20}O_2$ ($z = 0.08$)	0.34	0.37	0.02	0.98
$LiNi_{0.80}Fe_{0.20}O_2$ ($z = 0.14$)	0.34	0.38	0.01	1.10
$LiNi_{0.70}Fe_{0.30}O_2$	0.35	0.39	0.04	0.80
$LiNi_{0.40}Fe_{0.60}O_2$	0.35	0.56	0.003	0.95
α-$LiFeO_2$	0.38	0.69	0.003	0.78
$LiNi_{0.70}Fe_{0.30}O_2$	0.34	0.50	0.04	1.35
α-$NaFeO_2$	0.35	0.47	0.009	0.82

[a]IS is the isomer shift, $\overline{QS}$ is the average quadrupole splitting; Misfit gives the fraction of the signal that remains unfitted, and χ^2 represents the adequacy between the experimental and calculated data. Both the low Misfit values and χ^2 values close to 1 show the good agreement between the experimental and calculated data.[36]

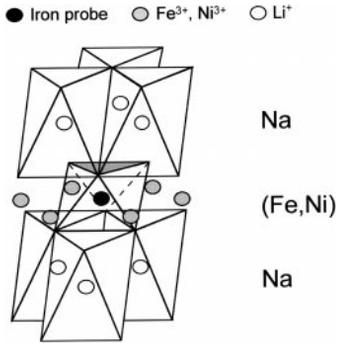

Fig. 8 Schematic representation of the cationic distribution around the $[FeO_6]$ octahedra in the layered $Na(Ni_{1-y}Fe_y)O_2$ phases.

ions (Ni,Fe) in the same slab and by three sodium ions in each adjacent sodium plane above and below the (Ni,Fe) slab. If the homologous lithium phase exhibits the same ideal structure, only one peak in the quadrupole splittings distribution is therefore expected.

Cubic phases

In the rocksalt type structure, there is only one type of cationic site from the crystallographic point of view. Nevertheless, at the local scale, various environments are expected depending on the topological distributions of Fe^{3+} and Li^+ ions. Indeed, the strong difference in ionic radii and in the ionic charges induces various electric field gradients which therefore lead to the peculiar distribution of discrete quadrupole splittings shown in Fig. 5. The octahedral linking is identical to that of the α-$NaFeO_2$ structure; the only difference results from the Li and Fe disordering. In Fig. 9, only the oxygen octahedron surrounding the iron probe has been drawn with various distributions of the first cationic neighbors given as example. Among them, the one represented in Fig. 9f is very similar to the cationic distribution found in α-$NaFeO_2$. Therefore, it must lead to the population of quadrupole splittings with a value close to 0.4. Other cationic distributions which are less isotropic must lead to higher values of the quadrupole splitting.

Layered $Li_{1-z}(Ni_{1-y}Fe_y)_{1+z}O_2$ $(0<y\leqslant 0.30)$ phases

A general comparison of the quadrupole splitting distributions suggests that the first population at the lower QS value is due to the iron ions localized within the (Ni,Fe)O_2 slabs (Fig. 10a). Concerning the second population of quadrupole splittings which appears when the amount of iron increases (Fig. 5) and especially when there is a large amount of transition metal ions

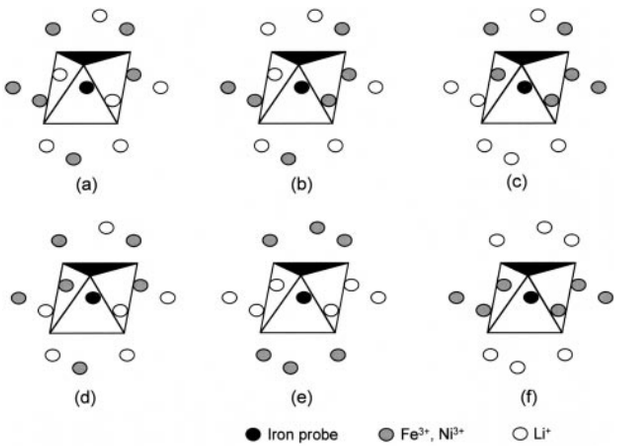

Fig. 9 Schematic representation of possible cationic distributions around $[FeO_6]$ octahedra in the cubic $Li(Ni_{1-y}Fe_y)O_2$ phases.

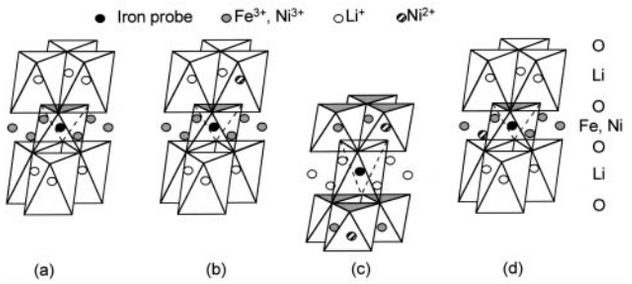

Fig. 10 Schematic representation of possible cationic distributions around $[FeO_6]$ octahedra in the layered $Li_{1-z}(Ni_{1-y}Fe_y)_{1+z}O_2$ phases.

in the interslab space (Fig. 6), several cationic distributions must be considered, as follows.

Presence of one Ni^{2+} ion in the vicinity of an iron ion. This nickel ion can be either in the slab (Fig. 10d) or in the interslab space (Fig. 10b). This first hypothesis does not seem to be valid since no second distribution appears in the case of the $Li_{0.94}(Ni_{0.90}Fe_{0.10})_{1.06}O_2$ phase which presents only one quadrupole splitting population in the presence of 12% of Ni^{2+} ions. Moreover, in the case of the $Li_{0.86}(Ni_{0.80}Fe_{0.20})_{1.14}O_2$ phase which contains 28% of Ni^{2+} ions, almost all iron ions statistically have one Ni^{2+} ion in their vicinity. Therefore, in this hypothesis, the second population of $\overline{QS}$ would be predominating. However, experimentally, in this latter material, the number of iron atoms involved in the second population is only about 1/3 of that involved in the first one.

Presence of lithium ions in the (Ni,Fe)O_2 slabs. This distribution, which would lead to a large QS value, is not considered likely to occur since the neutron diffraction study has shown that the amount of lithium ions in the slab was almost negligible even for materials with a large departure from the ideal stoichiometry.

Presence of iron ions in the lithium site (Fig. 10c). In this third hypothesis, two simultaneous effects contribute to the quadrupole splitting: (i) the presence of two divalent nickel ions of the (Ni,Fe)O_2 slabs in the vicinity of an iron ion to compensate for the excess of positive charge, (ii) very large C_{3v} distortion of the octahedron due to the presence of edge-sharing $[LiO_6]$ octahedra around the $[FeO_6]$ one. Indeed, the values of the O–M–O angles for the two types of octahedra in the structure, the one located in the lithium layer and the other in the nickel layer, represented in Fig. 11 and reported in Table 6, show that the $[FeO_6]$ octahedra in the interslab space are elongated along the c axis whereas the $[FeO_6]$ octahedra in the slab are contracted along this same axis. Moreover, if one considers the effect of (Ni,Fe) first cationic neighbors (Fig. 10a and c) two different environments are evidenced for iron ions which lead to two distinct average QS values. Note that most important is the deviation of the O–M–O angle from its theoretical value (90°), the more distorted are the octahedra, and the more the $\overline{QS}$ value increases. This does not explain why the average

Table 6 Values of the O–M–O (M = Fe, Ni) and O–A–O (A = Li, Na) angles for the two types of octahedra in the rhombohedral structure

	O–M–O (°) angles of the $[MO_6]$ (M = Ni, Fe) octahedra in the slab		O–M–O (°) angles of the $[AO_6]$ (A = Na, Li) octahedra in the interslab space	
	α_1	α_2	β_1	β_2
$Li_{0.94}(Ni_{0.90}Fe_{0.10})_{1.06}$	86.5	93.5	93.9	86.1
α-$NaFeO_2$	85.8	94.2	100.1	79.9

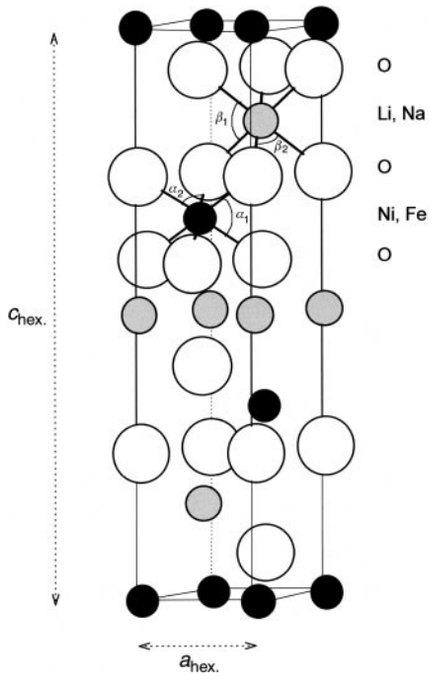

Fig. 11 Hexagonal cell representation of the rhombohedral $A(M)O_2$ structures (A = Li, Na; M = Ni, Fe). α_1 and α_2 are the O–M–O angles. β_1 and β_2 are the O–A–O angles.

quadrupole splitting values of the sodium phases are higher than those of the lithium phase (first peak at lower value) because the O–M–O angles in these two phases are very similar. However, one must notice that the difference in size and ionic character between lithium and sodium could influence the electric field gradient around iron ions and contribute to the variation of the $\overline{QS}$ value. Therefore, one can assume that the second population of quadrupole splittings results from the presence of iron ions in the lithium site.

This result is in agreement with those reported by Reimers *et al.* who have used anomalous X-ray scattering to discriminate between iron and nickel ions. They studied phases containing 20 and 23% iron; iron poorer phases could not be observed because of the sensitivity limits of the technique. However, they showed that iron atoms tend to occupy predominantly sites in the Li layers. Among various studies on similar iron substituted lithium cobaltite phases,[33–35] Kanno *et al.*, using Mössbauer spectroscopy, assumed that only a part of the iron ions are in the diamagnetic cobalt layer.[35] Indeed, Mössbauer spectra of these single phases have been fitted by at least two doublets with the same isomer shift and different quadrupole splittings indicating a QS distribution for each iron-doped sample.

Conclusion

The XRD study on the "$LiNi_{1-y}Fe_yO_2$" system for $0 < y \leqslant 1$ shows the existence of three domains ($y \leqslant 0.30$, lamellar phases; $y > 0.50$, cubic phases; $0.30 < y < 0.50$, coexistence of the lamellar and cubic phases) in agreement with Reimers *et al.* However, Mössbauer spectroscopy is a valuable tool for studying the small scale structure of $Li_{1-z}(Ni_{1-y}Fe_y)_{1+z}O_2$ for $z \leqslant 0.30$. Indeed, since the quadrupole splitting is very sensitive to the local environments of the iron atoms, Mössbauer spectroscopy allows one to clearly establish, comparing the lithium layered phases to the strictly 2D sodium reference ones, the cationic distribution around iron ions.

Since lamellar phases are interesting from the electrochemical point of view, their behavior upon cycling will be studied in a further paper.

Acknowledgements

The authors wish to thank M. Basterreix for technical assistance, P. Gravereau and M. Ménétrier for fruitful discussions, ILL for the neutron diffraction facilities, Région Aquitaine and CNES for financial support.

References

1 C. Delmas, I. Saadoune and A. Rougier, *J. Power Sources*, 1993, **43–44**, 595.
2 E. Zhecheva and R. Stoyanova, *Solid State Ionics*, 1993, **66**, 143.
3 A. Ueda and T. Ohzuku, *J. Electrochem. Soc.*, 1994, **141**, 2010.
4 E. Rossen, C. D. W. Jones and J. R. Dahn, *Solid State Ionics*, 1992, **57**, 311.
5 Y. Nitta, K. Okamura, K. Haraguchi, S. Kobayashi and A. Ohta, *J. Power Sources*, 1995, **54**, 511.
6 A. Rougier, Thesis, University of Bordeaux I, 1995.
7 J. N. Reimers, E. Rossen, C. D. Jones and J. R. Dahn, *Solid State Ionics*, 1993, **61**, 335.
8 R. Kanno, T. Shirane, Y. Inaba and Y. Kawamoto, *J. Power Sources*, 1997, **68**, 145.
9 A. Rougier, I. Saadoune, P. Gravereau, P. Willmann and C. Delmas, *Solid State Ionics*, 1996, **90**, 83.
10 I. Saadoune and C. Delmas, *J. Mater. Chem.*, 1996, **6**, 193.
11 T. Ohzuku, A. Ueda and M. Kouguchi, *J. Electrochem. Soc.*, 1995, **142**, 4033.
12 Q. Zhong and U. Von Sacken, *J. Power Sources*, 1995, **54**, 221.
13 C. Pouillerie, L. Croguennec, P. Biensan, P. Willmann and C. Delmas, *J. Electrochem. Soc.*, 2000, **147**, 2061.
14 D. Caurant, N. Baffier, B. Garcia and J. P. Pereira-Ramos, *Solid State Ionics*, 1996, **91**, 45.
15 Y. Takeda, J. Akagi, A. Edagawa, M. Inagaki and S. Naka, *Mater. Res. Bull.*, 1980, **15**, 1167.
16 J. Rodriguez-Carvajal, *Satellite Meeting on Powder Diffraction of the XV Congress of the IUCr*, Toulouse, France, 1990, p. 127.
17 M. Brunel and F. De Bergevin, *J. Phys. Chem. Solids*, 1969, **30**, 2011.
18 D. E. Cox, G. Shirane, P. A. Flinn, S. L. Ruby and W. J. Takei, *Phys. Rev. B*, 1963, **132**, 1547.
19 J. M. Cowley, *Acta Crystallogr., Sect. A*, 1973, **29**, 537.
20 J. J. Braconnier, Thesis, University of Bordeaux I, 1983.
21 L. Demourgues-Guerlou, J. J. Braconnier and C. Delmas, *J. Solid State Chem.*, 1993, **104**, 359.
22 Y. Takeda, K. Nakahara, M. Nishijima, N. Imanishi, O. Yamamoto, M. Takano and R. Kanno, *Mater. Res. Bull.*, 1994, **29**, 659.
23 A. Rougier, P. Gravereau and C. Delmas, *J. Electrochem. Soc.*, 1996, **143**, 1168.
24 R. D. Shannon and C. T. Prewitt, *Acta Crystallogr., Sect. B*, 1969, **25**, 925.
25 C. Pouillerie, E. Suard and C. Delmas, *Solid State Ionics*, submitted.
26 I. J. Pickering, J. T. Lewandowski, A. J. Jacobson and J. Goldstone, *Solid State Ionics*, 1992, **405**, 53.
27 J. B. Goodenough, D. G. Wickahm and W. J. Croft, *J. Appl. Phys.*, 1958, **29**, 382.
28 A. L. Barra, G. Chouteau, A. Stepanov, A. Rougier and C. Delmas, *Eur. Phys. J. B*, 1999, **7**, 551.
29 A. Hirano, R. Kanno, Y. Kawamoto, Y. Takeda, K. Yamaura, M. Takano, K. Ohyama, M. Ohashi and Y. Yamaguchi, *Solid State Ionics*, 1995, **78**, 123.
30 A. Rougier, C. Delmas and G. Chouteau, *J. Phys. Chem. Solids*, 1996, **57**, 1101.
31 T. Shirakami, M. Takematsu, A. Hirano, R. Kanno, K. Yamaura, M. Takano and T. Atake, *Mater. Sci. Eng. B*, 1998, **54**, 70.
32 D. Mertz, Y. Ksari, F. Celestini, J. M. Debierre, A. Stepanov and C. Delmas, *Phys. Rev. B*, 2000, **61**, 1240.
33 R. Alcantara, P. Lavela, J. L. Tirado, C. Pérez-Vicente, J. C. Jumas and J. Olivier-Fourcade, *Extended Abstract of the 9th International Meeting on Lithium Batteries, Edinburgh, 12–17 July 1998*, Poster II, Thur 16.
34 H. Sakaebe, M. Tabuchi, M. Shikano, H. Shunichi and T. Sakai, *Extended Abstract of the 9th International Meeting on Lithium Batteries, Edinburgh, 12–17 July 1998*, Poster II, Thurs 106.
35 M. Tabuchi, K. Ado, H. Kobayashi, H. Sakaebe, H. Kageyama, C. Masquelier, M. Yonemura, A. Hirano and R. Kanno, *J. Mater. Chem.*, 1999, **9**, 199.
36 S. L. Ruby, in *Mössbauer effect methodology*, ed. I. J. Gruverman, C. W. Seidel, New York, 1973, vol. 8, p. 263.